Asphyxia-activated corticocardiac signaling accelerates onset of cardiac arrest

Duan Li[a], Omar S. Mabrouk[b,c], Tiecheng Liu[a], Fangyun Tian[a], Gang Xu[a], Santiago Rengifo[a], Sarah J. Choi[b], Abhay Mathur[a], Charles P. Crooks[a], Robert T. Kennedy[b,c], Michael M. Wang[a,d,e,f,g], Hamid Ghanbari[f,h,i], and Jimo Borjigin[a,d,e,f,i,1]

Departments of [a]Molecular and Integrative Physiology, [b]Chemistry, [c]Pharmacology, [d]Neurology, and [h]Internal Medicine-Cardiology, [e]Neuroscience Graduate Program, [f]Cardiovascular Center, and [i]Michigan Center for Integrative Research in Critical Care, University of Michigan, Ann Arbor, MI 48109; and [g]Veterans Administration Ann Arbor Healthcare System, Ann Arbor, MI 48105

Edited by Solomon H. Snyder, Johns Hopkins University School of Medicine, Baltimore, MD, and approved March 16, 2015 (received for review December 14, 2014)

The mechanism by which the healthy heart and brain die rapidly in the absence of oxygen is not well understood. We performed continuous electrocardiography and electroencephalography in rats undergoing experimental asphyxia and analyzed cortical release of core neurotransmitters, changes in brain and heart electrical activity, and brain–heart connectivity. Asphyxia stimulates a robust and sustained increase of functional and effective cortical connectivity, an immediate increase in cortical release of a large set of neurotransmitters, and a delayed activation of corticocardiac functional and effective connectivity that persists until the onset of ventricular fibrillation. Blocking the brain's autonomic outflow significantly delayed terminal ventricular fibrillation and lengthened the duration of detectable cortical activities despite the continued absence of oxygen. These results demonstrate that asphyxia activates a brainstorm, which accelerates premature death of the heart and the brain.

asphyxic cardiac arrest | autonomic nervous system | coherence | directed connectivity | near-death experience

Sudden cardiac arrest occurs in more than 400,000 Americans annually, with a high rate of mortality. Fatal cardiac arrhythmias and sudden unexpected death occur in patients with cardiovascular disease (1) as well as those with no known history of heart disease (2–4). This latter class of patients includes individuals with ischemic stroke, traumatic brain injury, brain hemorrhage, epilepsy, and asphyxia. The physiological progression of a healthy heart to death is not well understood.

Asphyxia-induced cardiac arrest occurs in patients with airway obstruction, respiratory failure, pulmonary embolism, gas poisoning, drowning, and choking. Experimental asphyxia in animal models results in cardiac arrest within a few minutes. In all cases following the onset of asphyxia, electroencephalogram (EEG) amplitudes become extremely low before the disappearance of electrocardiogram (EKG) signals (5–8). Although no reports of EEG and EKG recordings are available from asphyxia in humans, loss of external consciousness and sensory responsiveness is often the first sign of clinical cardiac arrest and always precedes the termination of all cardiac electrical signals. Whether the extremely low levels of EEG signals at near death can support meaningful brain functions including internal states of consciousness has not been investigated until recently. Previously, we have found that the mammalian brain is surprisingly highly aroused within a few seconds of asphyxia despite nearly isoelectric intracortical EEG signals (9). The functional role of the highly coherent cerebral activity in the dying animals is unknown. One possibility is that the near-death cortical activation represents a homeostatic mechanism of the brain that serves to revive vital functions in the dying animals.

Circadian and emotional regulation of cardiac output is controlled by the central nervous system. Fluctuations in heart rate are mediated by autonomic input, with parasympathetic suppression and sympathetic elevation of heart rate (10). Parasympathetic suppression of heart rate is mediated by the synaptic release of acetylcholine from vagus nerve terminals, whereas sympathetic elevation of heart rate is mediated by norepinephrine release controlled by the neural signals traveling down the spinal cord from the brainstem. Sudden death induced by a life-threatening stressor is postulated to result from a generalized sympathetic storm within the autonomic nervous system (3). Consistent with this view, exposure to carbon dioxide leads to an immediate systemic surge of neurally released norepinephrine in the asphyxic rats (11); human patients with sustained ventricular arrhythmias exhibit higher levels of plasma norepinephrine levels (12). Despite the hypothesized role of brain–heart connections in sudden death, however, simultaneous and detailed analysis of the dying brain and heart has not been reported.

Brainstem nuclei mediate reflex control of the autonomic nervous system (13). Stimulation of locus coeruleus neurons, the site of norepinephrine synthesis critical in generating alertness, leads to activation of GABAergic neurotransmission and inhibition of parasympathetic cardiac vagal neurons via the activation of brainstem adrenergic receptors (14). Overexpression of a serotonin receptor in raphe nuclei results in sporadic autonomic crises including bradycardia (15). In addition to

Significance

How does the heart of a healthy individual cease to function within just a few minutes in the absence of oxygen? We addressed this issue by simultaneously examining the heart and the brain in animal models during asphyxiation and found that asphyxia markedly stimulates neurophysiological and neurochemical activities of the brain. Furthermore, previously unidentified corticocardiac coupling showed increased intensity as the heart deteriorated. Blocking efferent input to the heart markedly increased survival time of both the heart and the brain. The results show that targeting the brain's outflow may be an effective strategy to delay the death of the heart and the brain from asphyxia.

Author contributions: M.M.W. and J.B. conceived the project; D.L. and J.B. planned experiments and analysis; D.L. and G.X. wrote analysis programs; D.L., F.T., G.X., and S.R. analyzed data; O.S.M. and R.T.K. conceived the high-resolution analysis of brain neurochemicals; O.S.M. and S.J.C. performed liquid chromatography-mass spectrometry analysis of brain dialysates; T.L., G.X., and A.M. constructed electrodes; T.L. performed surgical implantation of all electrodes and microdialysis probe; T.L., A.M., C.P.C., and J.B. collected electroencephalogram, electrocardiogram, and electromyogram data; O.S.M., T.L., and S.J.C. conducted cortical microdialysis and sample collection; D.L. and G.X. wrote analysis program for electrocardiomatrix construction; H.G. assisted with validation of cardiac arrhythmias; and M.M.W. and J.B. wrote the paper.

Conflict of interest statement: The electrocardiomatrix technology used in the study to analyze heart signals is pending for patent protection.

This article is a PNAS Direct Submission.

[1]To whom correspondence should be addressed. Email: borjigin@umich.edu.

This article contains supporting information online at www.pnas.org/lookup/suppl/doi:10.1073/pnas.1423936112/-/DCSupplemental.

autonomic control, brainstem nuclei mediate a relay of cardiac (and other visceral) information to higher brain regions (13). A hierarchy of representations of cardiac function has been traced from brainstem to anterior cingulate and insular cortices, where conscious awareness of heartbeat is associated with enhanced cortical activity (16, 17). In patients with cardiac disease, heartbeat-evoked potentials are detectable in multiple cortical loci within the left hemisphere that reflect the proarrhythmic status of the heart (18).

The emerging theme from these and other studies supports the notion that the autonomic nervous system is under constant surveillance by the cerebral cortex to ensure functional integrity of vital organs. A life-threatening crisis of the heart, with a rapid and steep change of the heart rate and reduction of cardiac output, is therefore expected to markedly activate and recruit the cerebral cortex to form a hierarchical circuit of cardiac survival. When transient homeostatic feedback from the brain to the heart is insufficient to restore cardiac function, the brain may exhibit a sustained activation such that it may cause a premature and rapid death of the heart. In this paper, we examined cardiac and cortical responses to asphyxia by examining beat-to-beat changes of cardiac electrical signals, measuring brain neurotransmitter levels, analyzing cardiac event-related potentials, and calculating corticocortical/corticocardiac coherence and connectivity in dying animals. We also tested the effect of decentralization of the heart on lethal cardiac arrhythmias and brain electrical activity during asphyxia.

Results

A Marked Fluctuation of Heart Rate Dominates the Early Period of Asphyxia. To determine the time course of cardiac responses to asphyxia, we monitored EKG signals in rats during wakefulness and following carbon dioxide inhalation. The time course of EKG changes in a typical rat (ID5768; Fig. 1) shows that the amplitude of raw EKG signals declined gradually until asystole was observed 320 s later (Fig. 1*A*). Heart rate changes exhibited four distinct phases (Fig. 1 *B* and *C*): asphyxia phase I (A1; 3–25 s) consisted of a marked fluctuation of heart rate displaying an initial steep decline (3–10 s) followed by a rapid recovery (10–25 s). Asphyxia phase II (A2; 25–50 s) consisted of a second steep decline of heart rate, whereas phase III (A3; 50–265 s) was dominated by a low but stable heart rate of 1–2 Hz. During phase III, the heart rate continued to exhibit a mild fluctuation of ±0.5 Hz between the peak and the trough. Phase IV (A4; 265–320 s) was dominated by a fast heart rate that fluctuated between 9 and 15 Hz. The phase I response was robust in 8/10 rats and nearly undetectable in 2/10 rats (ID5745 and ID5769), whereas the phase II–IV responses were reproducible in all rats, although there was slight variation in the length for phases III and IV segments (Fig. S1).

Cardiac Electrical Signals, Visualized by Electrocardiomatrix, Reveal Temporally Distributed Cardiac Arrhythmias During Asphyxia. EKG signals exhibit a dynamic and ordered sequence of arrhythmias during asphyxia. To visualize the beat-to-beat features of cardiac signals monitored over a long period, we developed a new method of displaying long streams of EKG signals, called the electrocardiomatrix (ECM) (Fig. S2). The ECM graphs two or more consecutive P-QRS-T waves on the *y* axis, the numbers of heartbeats or time lapsed on the *x* axis, and signal intensity of heartbeats on the *z* axis. This display method preserves all features of cardiac electrical signals decipherable from raw EKG data in a compact manner and permits a single-glance view of time-dependent changes of heart rate and the occurrence of cardiac arrhythmias.

As shown in Fig. 1*D*, *a*, the beat-to-beat changes of cardiac electrical activity, displayed on the ECM, captured the RR interval (RRI) changes shown in Fig. 1*C* and identified all relevant cardiac features. Asphyxia-induced cardiac demise begins with a rapid induction of cardiac arrhythmias (2–16 s) followed by alternating sinus rhythm and second-degree heart block (Mobitz type II) (16–20 s) before reaching a brief restoration of RRI (20–30 s; Fig. 1*D*, *b* and *c*). This short recovery phase is marked by sinus rhythm with an ectopic peak and a premature ventricular beat (Fig. 1*D*, *c*). The transition to further rhythm deterioration begins with several consecutive beats of Mobitz II type (Fig. 1*D*, *c*) followed by unstable (32–37 s; Fig. 1*D*, *c*) and stable (37–90 s; Fig. 1*D*, *c* and *d*) third-degree atrioventricular block with junctional escape rhythms. This period of relative stability is terminated by another segment of cardiac turbulence, which contains alternating junctional and ventricular escape beats (90–120 s; Fig. 1*D*, *d*). During this period, RRIs showed another round of prolongation (decreasing heart rate; 80–95 s) and shortening (increasing heart rate; 95–125 s). Cardiac rhythms then transitioned completely from junctional escape beats to ventricular escape beats (or idioventricular rhythms) with a slowly declining heart rate

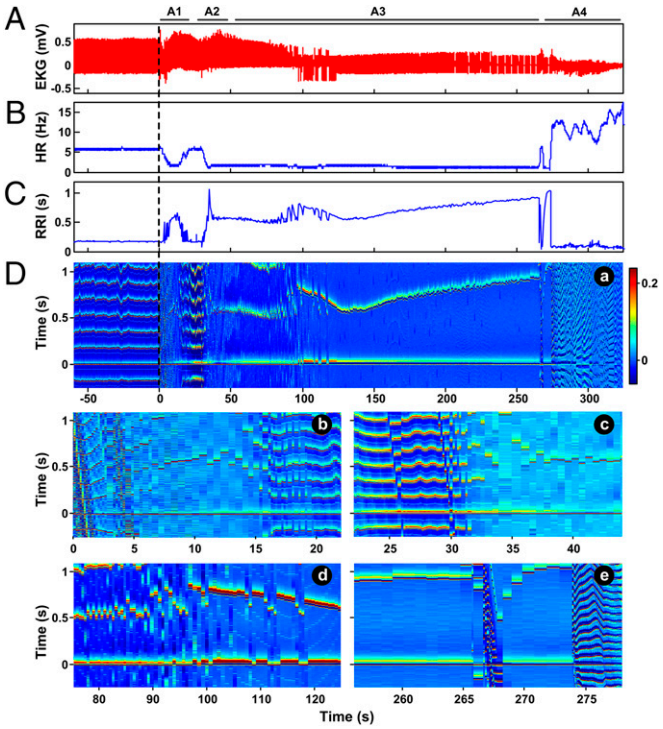

Fig. 1. Asphyxia results in a marked fluctuation of heart rate and stimulates temporally distributed and well-defined sequence of cardiac arrhythmias. (*A*) Carbon dioxide administration at time 0 leads to a gradual decline of the amplitude of EKG signals. Representative data from one adult outbred Wistar rat (ID5768) are shown. (*B*) Heart rate (HR) changes during asphyxia-induced cardiac arrest. Heart rate data were obtained from a 10-s epoch of EKG data with 9.9 s of overlap between two consecutive values. (*C*) Time intervals between two consecutive QRS complexes (RRIs) over the course of asphyxia. Asphyxia-induced cardiac failure progressed in four distinct phases (asphyxia stages 1–4, or A1–A4), as labeled on top of *A*. RRIs of all rats showed similar lawful progression of changes from A1 to A4 (Fig. S1). In two rats (ID5745 and ID5769), RRI changes in A1 phase were not as dramatic as in other rats. (*D*) ECM display of the EKG signals shown in *A*. The method of the ECM construction is detailed in *SI Text* and Fig. S2. Time-dependent features of P-QRS-T complexes of two or more consecutive heartbeats are displayed in *y* axis with amplitude of each peak (P, QRS, T) represented in Z-domain in color. Warmer color denotes higher signal strength. During baseline (–60 s to 0 s; *D*, *a*), eight consecutive QRS complexes are shown vertically in time domain with their R peak displaying the highest voltage (warmest color). Consecutive R peaks aligned at time 0 s in *x* axis expand horizontally with the P waves situated below the R-peak line and the T waves immediately above the R-peak line. Changes in the RRIs and intervals between various peaks and changes in the amplitude are readily apparent. Transitions between critical phases in *D*, *a* are further expanded in *D*, *b*–*e*.

(Fig. 1*D*, *a* and *d*). Toward the end of the idioventricular rhythm period, the rhythmic and dissociated P waves were mixed with and eventually replaced by fast fluttering and low-amplitude atrial rhythms (Fig. 1*D*, *e*). The bradyarrhythmia period (32–265 s) was followed by polymorphic ventricular tachycardia rhythms (274–320 s; Fig. 1*D*, *a* and *e*), which degenerated subsequently into ventricular fibrillation. Asystole was reached 400 s after the onset of asphyxia in this animal.

As in the case of heart rate changes, the progression of ECM-derived electrical profiles during asphyxia is conserved in all rats. The second drop in heart rate (or rise in RRIs) in A2 occurred between 25 and 35 s of asphyxia in all rats, which paralleled precipitous drops in blood oxygen content measured by MouseOx. The heart rate during the period of bradyarrhythmia (mainly in A3) dropped to about 24% (±4%) of the baseline values and never dipped below 1 Hz. Ventricular tachycardia onset varied from 180 s to 340 s with some rats showing long pauses in their cardiac electrical signals during this period. All rats reached asystole within 6 min of asphyxia (Fig. S1).

Asphyxia Activates a Global Cortical Coherence That Persists Until the Onset of Ventricular Fibrillation. Previously, we have reported a marked and brief surge of cortical coherence induced by asphyxia in anesthetized rats (9). A robust increase of global coherence induced by carbon dioxide inhalation is evident in the absence of anesthesia and progresses with a temporally well-defined sequence (Fig. 2). The mean coherence, measured by averaging all pairwise coherence values between six cortical sites (left and right frontal lobes, left and right parietal lobes, and left and right occipital lobes), increased immediately following the onset of asphyxia for gamma bands above 150 Hz and for the theta band (5–10 Hz). In addition, a cluster of increased coherence within the gamma-2 frequency band (65–115 Hz) is prominent during A1 (defined above) phase, whereas a cluster of increased coherence within gamma-1 (25–55 Hz) dominates the A2 phase (Fig. 2*A*). The gamma band clusters at 100 Hz and 50 Hz coincide with the two phases of steep RRI changes: the 100-Hz cluster occurs during A1 (when RRI increases from 0.18 s to 0.63 s), and the 50-Hz cluster occurs during A2 (when RRI increases from 0.18 s to 1.1 s to 0.58 s). Both clusters of coherence were diminished during the period of transient recovery of heart rate that lasted for just a few seconds (between A1 and A2). During the third phase of asphyxia (A3) when RRI hovers between 0.5 and 1 s (heart rate of 1–2 Hz; bradyarrhythmia with complete heart block), cortical signals showed intense coherent activities at lower-frequency ranges, mostly below 50 Hz (100–280 s after asphyxia in Fig. 2*A*). Cortical coherence exhibited altered temporal patterns during ventricular tachycardia (A4) and declined precipitously at the onset of ventricular fibrillation.

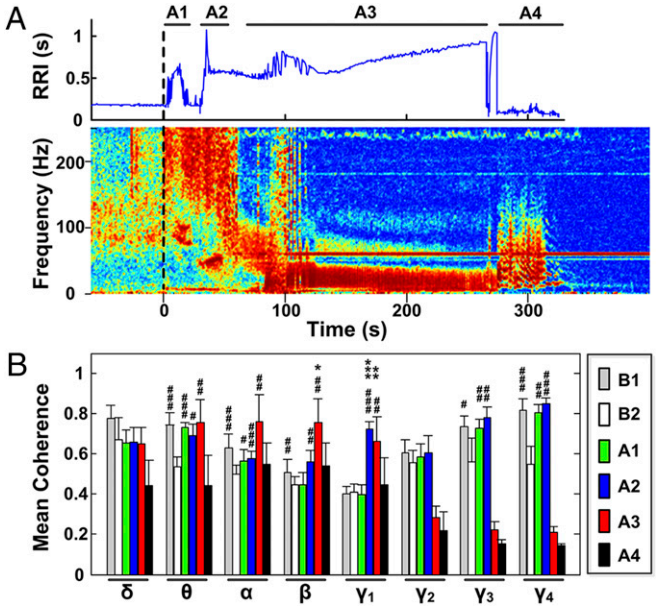

Fig. 2. Corticocortical coherence, stimulated by asphyxia, persists until the onset of ventricular fibrillation. (*A*) Mean cortical coherence values, averaged over the six EEG channels before and following the onset of asphyxia at time 0, were measured in 2-s bins with 1 s overlap. Coherence showed cardiac stage-specific features (indicated by the change of RRI above the coherence plot from the same animal, ID5768). In both A1 and A2, a marked elevation of high-frequency coherence (gamma-3, 125–175 Hz; gamma 4, 185–235 Hz) and theta (5-10 Hz) coherence was evident. In addition, a cluster of gamma-2 (65–115 Hz) coherence centered at 100 Hz was prominent in A1, whereas a cluster of gamma-1 (25–55 Hz) coherence centered at 50 Hz was distinct in A2. During A3, cortical coherence transitioned to lower-frequency range and persisted below 50 Hz for the later A3 stage. During A4, coherence was found above theta and below gamma-3 waves with altered patterns. An intense band at 60 Hz and a faint band at 180 Hz were generated by ambient electromagnetic noise and persisted for as long as recording continued (30 min after asphyxia). (*B*) The mean and SD of EEG coherence computed for eight frequency bands at baseline of B1 (active waking period; Fig. S3), B2 (quiet waking period; Fig. S3), and A1–A4 states ($n = 10$). Significant change over B1 period is indicated using an asterisk over the data, whereas significant values over B2 period are marked by a pound sign. Error bars denote SD (*/$^{\#}P < 0.05$, **/$^{\#\#}P < 0.01$, ***/$^{\#\#\#}P < 0.001$).

Cortical Effective Connectivity Increases During Asphyxic Cardiac Arrest. Effective connectivity measures explore causal relationship between two or more connected neural networks (19). Feedback (frontal to parietal/occipital areas) and feedforward (occipital/parietal to frontal areas) connectivity analyses (9, 20) were applied to eight frequency bands in consecutive 2-s bins (Fig. 3). During A1 (see Fig. 3*A* for a representative rat), there was a marked surge of connectivity in theta band in both feedforward and feedback directions and a mild increase of connectivity for gamma-2, gamma-3, and gamma-4 bands. For the theta band, feedforward values were greater than that of the feedback. During A2, theta continued to exhibit higher levels of connectivity, and gamma-2 to gamma-4 bands also showed increased connectivity values. Gamma-1 band showed a marked increase in connectivity in both directions in A2. During A3, the increase in feedforward connectivity was seen for delta (0–5 Hz) broadly and for theta to gamma-1 bands during a restricted period (80–100 s). A mild increase in both feedback and feedforward connectivity was detected for theta, alpha, beta, and gamma-1 bands. During A4, a further surge of cortical connectivity was seen for alpha, beta, and gamma-1 bands (Fig. 3*A*).

Under baseline conditions, feedforward connectivity in the active B1 state was elevated in comparison with the quiet B2 state for the theta, alpha, beta, gamma-3, and gamma-4 bands, whereas feedback connectivity in the B1 state was significantly elevated over the B2 state for alpha, gamma-3, and gamma-4 bands (Fig. 3*B*). Theta connectivity in A1 showed a significant increase over B1 in both feedforward and feedback directions. A significant elevation of gamma-1 connectivity was detected in

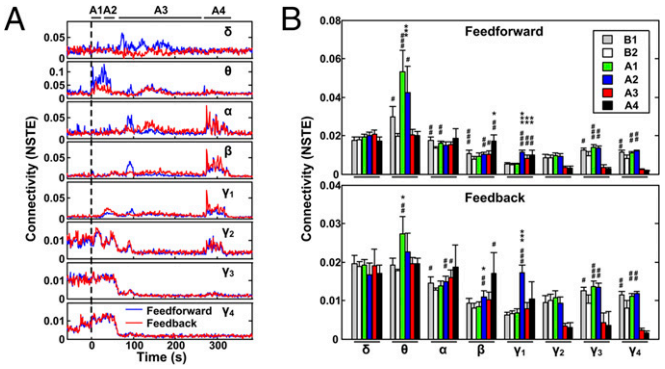

Fig. 3. Cortical connectivity surges following asphyxia onset. (*A*) Time course of cortical connectivity for the eight indicated bands 60 s before and 400 s after the onset of carbon dioxide asphyxia. Connectivity between frontal lobes and posterior areas was measured in 2-s bins with 1 s overlap using the NSTE technique. The vertical dashed bar denotes the onset of asphyxia. Cardiac stage (A1–A4, defined in Fig. 1) is indicated on top of the graph. (*B*) The average ($n = 10$) feedforward (*Upper*) and feedback (*Lower*) connectivity for all eight frequency bands during baseline (B1 and B2) and each of the cardiac stages (A1–A4) during asphyxia. Significant changes over the B1 period are indicated using an asterisk over the data, whereas significant values over B2 period are marked by a pound sign. Error bars denote SD ($*/\#P < 0.05$, $**/\#\#P < 0.01$, $***/\#\#\#P < 0.001$). A significant decline of connectivity index from A2 to A3 was detected for gamma bands ($P < 0.001$) in both directions and for theta band in feedforward direction ($P < 0.001$). Significant increase from A3 and A4 was seen for beta bands in both directions ($P < 0.01$) and feedforward direction for gamma-1 band ($P < 0.05$).

both feedforward and feedback directions during A2. During A1 and A2, gamma-3 and gamma-4 bands exhibited significant increase in connectivity in both directions compared with the B2 baseline. During A3, significant feedforward connectivity elevation was seen for beta and gamma-1 bands, whereas significant feedback connectivity elevation was seen for the alpha band. During A4, beta band connectivity showed increased values in both feedback (vs. B2) and feedforward (vs. B1 and B2) directions, whereas gamma-1 band showed significant connectivity elevation only in feedforward direction (vs. B1 and B2). Theta bands showed significantly higher feedforward connectivity than feedback connectivity during both A1 and A2 ($P < 0.001$), whereas gamma-1 showed higher levels in the feedback direction than in the feedforward direction ($P < 0.001$). When cardiac conditions worsened during A3 and A4 (progressing from bradyarrhythmia to ventricular tachycardia), cortical connectivity increased in the beta band in both feedback and feedforward directions ($P < 0.01$) and in the gamma-1 band in the feedforward direction ($P < 0.05$).

Asphyxia Stimulates a Rapid and Dramatic Release of Core Neurotransmitters in the Cerebral Cortex. To probe the neurochemical basis of the heightened cortical activities, we performed minute-by-minute microdialysis in the frontal and occipital lobes of unanesthetized rats ($n = 7$) before and during asphyxiation and analyzed cortical dialysates using liquid chromatography-mass spectrometry (LC-MS) (21). As expected, levels of brain glucose dropped rapidly in both frontal and occipital areas (Fig. 4*A*, *a*) and fell below 50% of the baseline values within 2 min of asphyxia (Fig. 4*A*, *b*). In both frontal and occipital cortices, a dramatic and significant surge of secretion was detected for as long as 20 min of asphyxia for all neurotransmitters tested (Fig. 4 *B*, *a* through *H*, *a*). As early as time 0, a significant elevation was already evident for dopamine (Fig. 4*C*), increasing an average of fourfold in both frontal and occipital lobes (4x/FL and 4x/OL; Fig. 4*C*, *b*), norepinephrine (12x/FL and 9x/OL; Fig. 4*E*, *b*), and GABA (8x/FL and 7x/OL; Fig. 4*F*, *b*). Within the first minute of asphyxia, a significant increase of release was found for adenosine (18x/FL and 26x/OL; Fig. 4*B*, *b*), glutamate (1.3x/FL and 1.2x/OL; Fig. 4*G*, *b*), aspartate (1.6x/FL and 1.4x/OL; Fig. 4*H*, *b*), and serotonin (13x/FL; Fig. 4*E*, *b*). By the second minute of asphyxia, serotonin release in occipital lobe began to show a significant increase (22x/OL; Fig. 4*E*, *b*). Compared with the occipital lobe, frontal lobe secretion is significantly higher for serotonin starting from the fourth minute (Fig. 4*E*, *b*) and for norepinephrine (Fig. 4*D*, *b*) beginning from the first minute of asphyxia. Adenosine (Fig. 4*B*, *b*) and dopamine (Fig. 4*C*, *b*) also exhibited higher levels of secretion in the frontal lobe than the occipital lobe. In contrast, GABA (Fig. 4*F*, *b*), glutamate (Fig. 4*G*, *b*), and aspartate (Fig. 4*H*, *b*) did not show regional differences in secretion following asphyxia. A temporal–spatial order of secretion was uncovered for several neurotransmitters: peak occipital secretory activity preceded frontal activity for adenosine (2 min/OL and 4 min/FL; Fig. 4*B*, *b*), norepinephrine (2 min/OL and 4 min/FL; Fig. 4*D*, *b*), and serotonin (4 min/OL and 5 min/FL). Although adenosine (Fig. 4*B*, *a*), dopamine (Fig. 4*C*, *a*), norepinephrine (Fig. 4*D*, *a*), and serotonin (Fig. 4*E*, *a*) secretion tapered after 3–5 min of asphyxia, levels of secretion continued to climb mildly for GABA (Fig. 4*F*, *a*), glutamate (Fig. 4*G*, *a*), and aspartate (Fig. 4*H*, *a*).

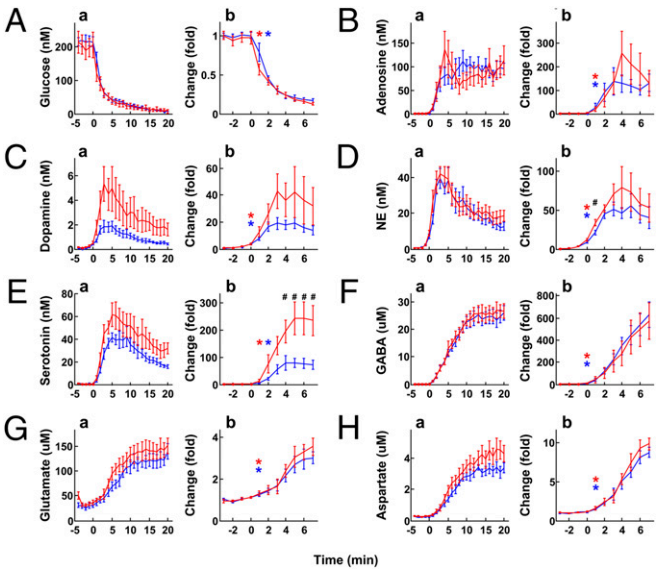

Fig. 4. Cortical neurotransmitter secretion shows immediate and marked surge in response to asphyxia. In *A*–*G*, concentration graph in nM or μM is shown in *a* for the entire sampling period (25 min), and normalized (to the baseline) graph in fold changes is shown in *b* for a total of 10 min. Glucose concentration showed marked decline in both frontal (red tracing) and occipital (blue tracing) areas (*A*). Extracellular concentrations of measured neurotransmitters, including adenosine (*B*), dopamine (*C*), norepinephrine (NE; *D*), serotonin (*E*), GABA (*F*), glutamate (*G*), and aspartate (*H*), all showed marked elevation in response to asphyxia ($n = 7$). In comparison with the baseline values, significant surge was detected as early as time 0 for dopamine, norepinephrine, and GABA in both frontal and occipital lobes. At 1 min of asphyxia, all seven neurotransmitters showed significant ($P < 0.05$) elevation in both cortical sites, except serotonin in occipital lobe, where significant elevation was found at 2 min of asphyxia. A significant ($P < 0.05$, $n = 7$) regional difference (frontal vs. occipital lobes) in the degree of elevation from baseline was found for serotonin at 4–7 min of asphyxia and for norepinephrine at 1 min, both of which were more elevated in the frontal areas than the occipital areas (*D*, *b* and *E*, *b*). Adenosine (*B*, *b*) and dopamine (*C*, *b*) also showed a similar trend. Error bars denote SEM. The first time point that shows significant elevation over baseline is marked by asterisks, with red indicating frontal cortex release and blue denoting occipital cortex secretion. The black pound signs in *D*, *b* and *E*, *b* indicate significant difference in release between the frontal and occipital cortices.

In addition to the neurotransmitters described above, acetylcholine, taurine, histamine, and glycine release was also significantly stimulated by asphyxia (Fig. S4 *A–D*). Glutamine and serine showed a mild elevation, whereas phenylalanine and tyrosine showed no change (Fig. S4 *E–H*). Dopamine metabolites, 3-MT (3-methoxytyramine) and DOPAC (3,4-dihydroxyphenylacetic acid), showed biphasic responses with increased 3-MT and decreased DOPAC concentration. The norepinephrine metabolite, NM (normetanorphrine), showed increased concentration, whereas the serotonin metabolite, 5-HIAA (5-hydroxyindoleacetic acid), displayed reduced levels (Fig. S4 *I–L*).

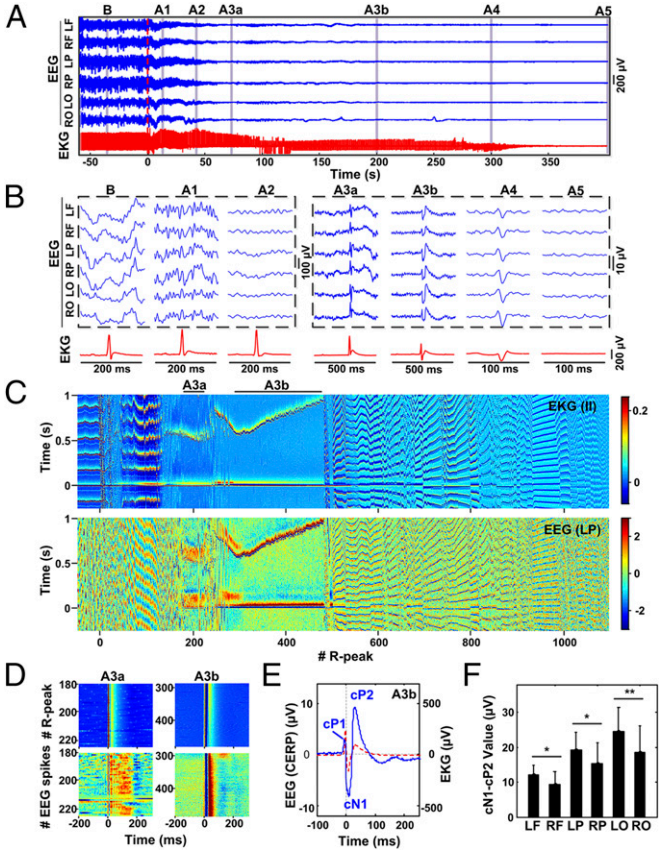

Fig. 5. Asphyxia stimulates a surge in cardiac event-related potential in cerebral cortices. (*A*) EEG raw signals (in blue tracings) from left frontal (LF), right frontal (RF), left parietal (LP), right parietal (RP), left occipital (LO), and right occipital (RO) lobes are displayed side by side with EKG signals (in red tracing) from the same animal (ID5768). The onset of asphyxia at time 0 s is marked by a red dashed line. (*B*) Short segments [at baseline (B) and at A1, A2, A3a, A3b, A4, and A5 stages] marked by gray vertical lines in *A* are further expanded for a more detailed look. (*C*) Matrix display of EKG (*Upper*) and EEG (*Lower*; LP) signals. The *x* axis is shown in numbers of QRS peaks (# R-peak). Color bars denote the signal strength in mV in EKG matrix and indicate normalized values in EEG matrix. (*D*) EKG and EEG matrices in A3a and A3b in *C* are further expanded and aligned top (EKG matrix) to bottom (EEG matrix) for a more detailed look. The EEG spikes that aligned with the heartbeats are termed "Cardiac Event-Related Potential (CERP)." (*E*) CERP obtained from 185 beats in A3b is averaged for one rat (in blue tracing) and displayed along with the averaged heartbeat (in red tracing) to show the general features. CERP amplitude is displayed using the left *y* axis, and heartbeat amplitude is according to the right *y* axis. Three prominent peaks in CERP are named as cardiac positive potential 1 (cP1), cardiac negative potential 1 (cN1), and cardiac positive potential 2 (cP2). (*F*) CERP difference between the cN1 and cP2 peaks (cN1 – cP2), computed for each cortical site in each rat ($n = 10$), shows marked left-right asymmetry. Error bars denote SD (*$P < 0.05$, **$P < 0.01$).

Asphyxia Activates Asymmetric Cardiac Event-Related Potentials in the Cerebral Cortex. Cortical coherence and directed connectivity both exhibited marked increase that paralleled the changes of cardiac rhythms (Figs. 1–3). This finding prompted us to examine the relationship between heart and brain electrical signals in detail. EEG signals collected from six cortical regions (left and right frontal lobes, left and right parietal lobes, and left and right occipital lobes) from a typical rat showed a rapid decline in amplitude within the first minute of asphyxia, whereas the EKG raw signals were readily visible for about 5 min (Fig. 5*A*). In an expanded view (Fig. 5*B*), stage-specific features of cortical signals become apparent: during the first minute of asphyxia (A1 and A2), the appearance of cortical oscillations underwent stage-specific changes in all channels (Fig. 5*B*, *Left*). No cardiac event-related potentials are detected during this period. When the EEG amplitude fell below 5% of the baseline levels during A3 phase, EEG signals were mixed with spikes that were synchronized with EKG peaks in all six cortical loci (Fig. 5*B*, *Right*). Disappearance of the cortical potential was in sync with the loss of all cardiac signals in A5 (asystole).

EEG raw signals from the left parietal lobe (normalized by subtracting the temporal mean and dividing by the temporal SD to facilitate the visual display of EEG morphology) were aligned to the heartbeat of the same rat to form an EEG matrix with methods used to generate ECM (Fig. S2) and were compared with the ECM from the same animal (Fig. 5*C*). EKG and EEG matrices had little similarity under baseline conditions (time before 0 s; Fig. 5*C*). Following the onset of asphyxia during A1, EEG signals underwent an intriguing series of oscillatory changes that maintained a dynamic phase relationship with heart rhythms (0 to 80th beat). During the temporary stabilization of the heart rate to baseline levels, the EEG signals exhibited prominent phase relations with the EKG (80th to 150th beat). The subsequent turbulence in cortical oscillations coincided with destabilized heart rhythms and a marked reduction of heart rate from 5.7 Hz to 1.6 Hz (150th to 180th beat). Following the steep fall of the heart rate, cortical signals became strongly synchronized with heartbeat rhythms and displayed cardiac event-related potential from the 185th EKG spike onward (Fig. 5*C*, *Lower*). The transition from junctional escape rhythms (A3a) to idioventricular rhythms (A3b) at the 310th heartbeat was associated with the change of cardiac event-related potential morphology in EEG signals (Fig. 5*C*). The morphological differences between the A3a and A3b were evident when EKG and EEG signals were placed side by side (Fig. 5*D*). With each junctional escape beat in A3a, cortical signals showed prolonged elevation of potential that lasted for more than 160 ms. This pattern was distinct from the cortical signals during the idioventricular rhythm period (A3b), which displayed a steep negative potential following each heartbeat and a marked elevation of a positive potential that lasted a short period (25–60 ms; Fig. 5*D*). The cardiac event-related potential during the A3b period lasted on average over 200 heartbeats, which exhibited a waveform of an event-related potential that included a cardiac positive peak 1 (cP1), negative peak 1 (cN1), and positive peak 2 (cP2; Fig. 5*E*). Cardiac event-related potential amplitude (defined as potential difference between cN1 and cP2 peaks) was significantly higher in the left hemisphere compared with the right hemisphere ($P < 0.05$ for all three pairs) and higher in the occipital cortex than parietal and frontal cortex (Fig. 5*F*; $n = 10$).

A Marked Surge of Corticocardiac Coherence Is Identified During Asphyxia Cardiac Arrest. The detection of cardiac event-related potentials (Fig. 5 *D–F*) prompted us to examine long-range coherence between the heart and the brain electrical signals during asphyxia. Although no detectable corticocardiac (between the cerebral cortex and the heart) coherence was found before asphyxia, high levels of brain–heart coherence were found in dying animals (Fig. 6). Corticocardiac coherence was undetectable during A1 and

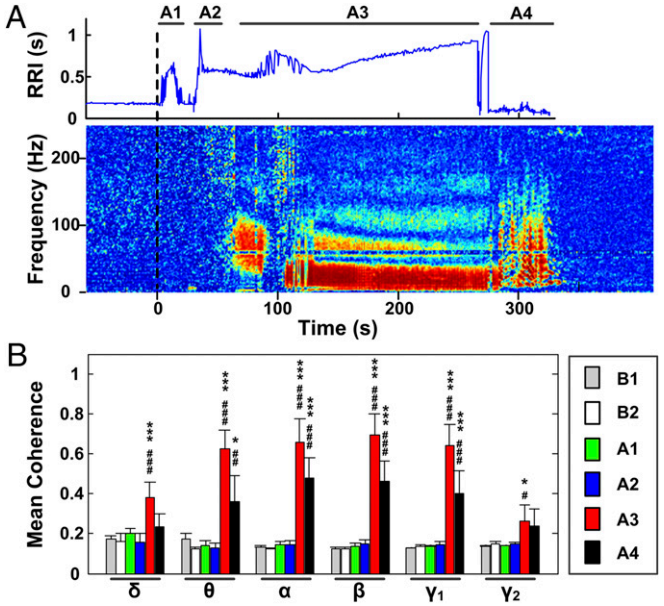

Fig. 6. Asphyxia activates corticocardiac coherence at near-death. (*A*) Brain–heart (corticocardiac) coherence, measured between the EKG signal and EEG signal from each of the six cortical sites at 2-s bins with 1 s overlap, shows a delayed surge. Corticocardiac coherence showed cardiac stage-specific features (ID5768). (*B*) The mean and SD of brain–heart coherence at B1 and B2 baseline (Fig. S3) and A1–A4 states (n = 10). Significant change over B1 period is indicated using an asterisk over the data, whereas significant values over B2 period are marked by pound signs. Error bars denote SD ($^{*/\#}P < 0.05$, $^{**/\#\#}P < 0.01$, $^{***/\#\#\#}P < 0.001$).

A2 (Fig. 6*A*). A surge of corticocardiac coherence emerged during the A3 period of bradyarrhythmia and persisted for as long as the heart was beating. The pattern of brain–heart coherence was distinct during early (50–80 s featuring junctional escape rhythms) and late (100–265 s with ventricular escape rhythms) A3. Corticocardiac coherence exhibited altered patterns during ventricular tachycardia (A4; Fig. 6*A*), which then declined precipitously at the onset of ventricular fibrillation (290 s).

The near-death surge of corticocardiac coherence was significant over B2 for the following frequency bands (Fig. 6*B*): delta, theta, alpha, beta, gamma-1, and gamma-2 during the period of complete heart block (A3) and theta, alpha, beta, and gamma-1 during the ventricular tachycardia period (A4). Compared with B1, significant levels of coherence were found for delta, theta, alpha, beta, gamma-1, and gamma-2 bands during A3 and for theta, alpha, beta, and gamma-1 waves during A4. Additional coherence elevation was found for gamma-1 during A1 and A2, relative to the active waking period. A significant elevation of corticocardiac coherence was also detected during the active waking period compared with the quiet waking in the theta band.

Asphyxia Activates Effective Connectivity Between the Cerebral Cortex and the Heart. Directed connectivity analyses (9, 20) were applied to the brain and heart electrical signals before and following asphyxia induction. Feedback (from each of the six cortical areas to the heart) and feedforward (from the heart to each of the six cortical sites) corticocardiac connectivity analyses were applied to six frequency bands in consecutive 2-s bins with 1 s overlap. A marked surge of corticocardiac directed connectivity was detected in both feedback and feedforward directions and exhibited frequency-dependent and cardiac stage-dependent changes during asphyxia (Fig. 7). A clear increase in both feedback and feedforward corticocardiac connectivity was evident in the theta band as early as during the transition from A1 to A2 (Fig. 7*A*). Elevated connectivity was also detected when cardiac conditions transitioned from the A2 to A3 for both delta and theta bands. During the late A3 period (100–265 s) when cardiac activity was dominated by idioventricular rhythms, a marked surge of feedback connectivity was evident for theta, alpha, and beta bands. When cardiac signals transitioned to ventricular tachycardia, a further surge of brain–heart connectivity was seen for low- as well as high-frequency bands (Fig. 7*A*). The onset of ventricular fibrillation invariably coincided with markedly diminished corticocardiac connectivity.

Compared with baseline, heart-to-brain (Fig. 7*B*, *Upper*) and brain-to-heart (Fig. 7*B*, *Lower*) effective connectivity values were significantly elevated for multiple frequency bands. In comparison with B1, a significant surge in heart-to-brain connectivity was found for theta in A4 and for alpha, beta, and gamma-1 in both A3 and A4. In comparison with B2, delta in A1, theta, alpha, beta, and gamma-1 in A3 and A4 showed significant elevation in feedforward corticocardiac connectivity (Fig. 7*B*, *Upper*). Unlike the feedforward direction where the significant levels of effective connectivity were detected mostly during the A3 (complete heart block) and A4 (ventricular tachycardia), feedback (from the brain to the heart) corticocardiac connectivity was significantly elevated as early as during A1 and A2 (vs. B2) for lower-frequency bands (delta, theta, and alpha). During the advanced stages of asphyxia in A3 and A4, the directed feedback corticocardiac connectivity surge was significantly higher for all frequency bands (Fig. 7*B*, *Lower*).

During asphyxia when heart signals transitioned from an incomplete heart block in A1 and A2 to complete heart block in A3, there is a marked and significant surge of feedback as well as feedforward connectivity between the brain and the heart for all frequency bands (A3 vs. A2: $P < 0.001$ for all frequencies). When asphyxia-induced cardiac failure progressed from A3 to A4, connectivity was decreased for low-frequency bands (delta and theta) but was strengthened significantly for higher-frequency bands (A4 vs. A3; beta: $P < 0.001$; gamma-1 and gamma-2: $P < 0.01$) in the feedback direction (Fig. 7*B*). Thus, corticocardiac directed

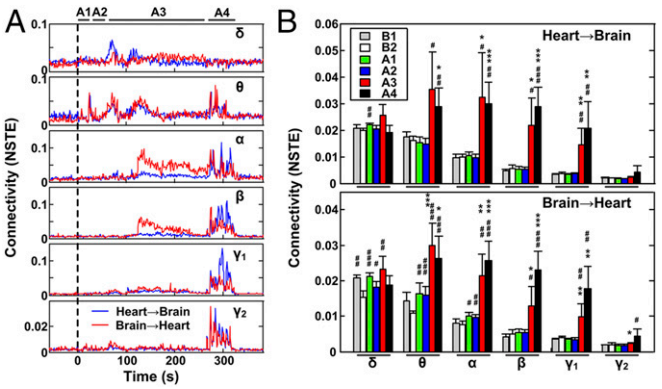

Fig. 7. Corticocardiac connectivity surges following asphyxia onset. (*A*) Corticocardiac connectivity for a typical rat (ID5768). Effective connectivity between the heart and each of the cortical sites was measured in 2-s bins with 1 s overlap using the NSTE technique. The vertical dashed bar denotes the onset of asphyxia. Cardiac stage (A1–A4, defined in Fig. 1) is labeled on top of the graph. The blue tracings mark the heart to brain (feedforward), and the red tracings mark the brain to heart (feedback) connectivity. (*B*) The average (n = 10) heart-to-brain (*Upper*) and brain-to-heart (*Lower*) connectivity during asphyxia. Significant changes over B1 are indicated using an asterisk over the data, whereas significant values over B2 are marked by a pound sign. A significant decline from A2 to A3 was detected for all gamma bands ($P < 0.001$) in both directions and for theta band in feedforward direction ($P < 0.001$). Significant increase from A3 and A4 was seen for beta bands in both directions ($P < 0.01$) and feedforward direction for gamma-1 band ($P < 0.05$). Error bars denote SD ($^{*/\#}P < 0.05$, $^{**/\#\#}P < 0.01$, $^{***/\#\#\#}P < 0.001$).

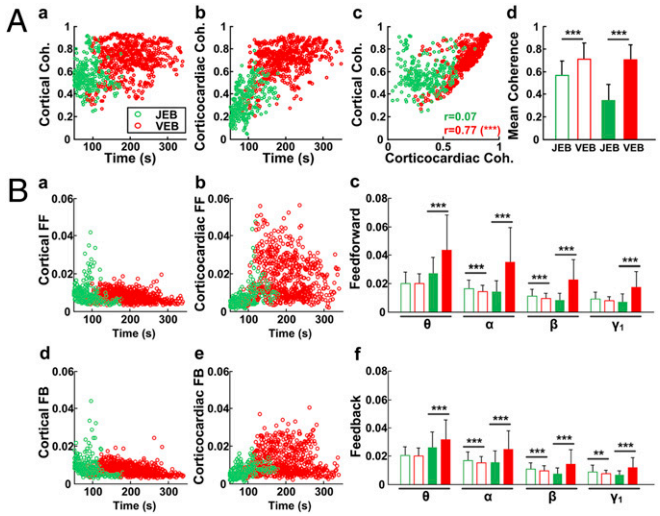

Fig. 8. Brain and heart electrical communication intensifies as cardiac conditions deteriorate during bradyarrhythmia. (*A*) Cortical and corticocardiac coherence (0.5–55 Hz), sorted according to the arrhythmia types in eight rats [complete heart block with junctional escape beats (JEB; green) or with ventricular escape beats (VEB; red)]. Each coherence data point (red or green circles) represents a nonoverlapping epoch of 2 s. Cortical (*A*, *a*) and corticocardiac (*A*, *b*) coherence in A3 data are displayed for JEB and VEB signals for eight rats. A linear correlation between the levels of cortical coherence and corticocardiac coherence was identified for ventricular beats (VEB; Spearman's r of 0.77, $P < 0.001$) (*A*, *c*). No such relationship was found for junctional beats (JEB; Pearson's r of 0.07) (*A*, *c*). Significantly higher coherence was found for VEBs within the brain (cortical coherence; open red bar) and between the heart and brain (corticocardiac; solid red bar) than for JEBs within the brain (open green bar) or between the heart and brain (solid green bar) ($P < 0.001$) (*A*, *d*). (*B*) Corticocardiac directed connectivity, sorted according to cardiac arrhythmia types (JEB and VEB; $n = 8$). Each connectivity data point (red or green circles) represents a nonoverlapping epoch of 2 s. Cortical feedforward (FF) connectivity (*B*, *a*), corticocardiac feedforward connectivity (*B*, *b*), cortical feedback connectivity (*B*, *d*), and corticocardiac feedback connectivity (*B*, *e*) were computed for the gamma-1 band for both JEB (green circles) and VEB (red circles). Cortical (*B*, *c*, open bars) and corticocardiac (*B*, *c*, solid bars) feedforward connectivity and cortical (*B*, *f*, open bars) and corticocardiac (*B*, *f*, solid bars) feedback connectivity were computed for other indicated frequency bands for both JEB (green bars) and VEB (red bars). Error bars denote SD (**$P < 0.01$, ***$P < 0.001$).

connectivity peaked during ventricular tachycardia for higher-frequency bands (beta, gamma-1, and gamma-2) and during bradyarrhythmia for lower-frequency bands (delta and theta).

Corticocardiac Connectivity Intensifies as Cardiac Functions Deteriorate During Asphyxic Cardiac Arrest. A3 stage of asphyxia-induced cardiac arrest was dominated by slow heartbeats with a complete heart block and sequential junctional and ventricular escape beats (Fig. 1). To determine the levels of corticocardiac connectivity during A3, we sorted cortical (Fig. 2) and corticocardiac (Fig. 6) coherence data (0.5–55 Hz) according to the type of cardiac arrhythmias the rats were exhibiting. As shown in Fig. 8*A*, junctional escape beats (JEB) were confined in all tested rats ($n = 8$) within early A3 (50–180 s), whereas ventricular escape beats (VEB) dominated the latter half of A3 (100–320 s; Fig. 8*A*, *a* and *b*). Higher levels of cortical coherence (Fig. 8*A*, *a*) and corticocardiac coherence (Fig. 8*A*, *b*) were associated with VEB than with JEB. A significant linear correlation ($P < 0.001$) was found between cortical coherence and corticocardiac coherence during ventricular escape rhythms (Fig. 8*A*, *c*). No such relationship existed during junctional escape rhythms. Coherence values during ventricular escape rhythm period were significantly higher both within the brain (cortical coherence) and between the brain and heart (corticocardiac coherence) than during junctional escape rhythms (Fig. 8*A*, *d*).

Effective connectivity within the brain and between the brain and heart were also analyzed during VEB and JEB in A3 (Fig. 8*B*). Feedforward connectivity for gamma-1 band within the brain (from parietal/occipital lobes to frontal lobes; Fig. 8*B*, *a*) showed a slightly higher value for junctional beats than for ventricular beats, whereas feedforward connectivity between the heart and brain (from the heart to each of the six cortical loci; Fig. 8*B*, *b*) was clearly higher with idioventricular rhythms than with junctional rhythms. The same was noted for theta, alpha, and beta bands (Fig. 8*B*, *c*). Within the brain, directed feedforward connectivity in alpha and beta bands was higher for junctional rhythms than for ventricular beats (Fig. 8*B*, *c*). Brain-to-heart feedback connectivity in the gamma-1 band clearly increased more during idioventricular rhythms than during junctional beats (Fig. 8*B*, *e*), whereas slightly higher values were detected during junctional escape beats for cortical feedback connectivity than for ventricular beats (Fig. 8*B*, *d*). A significant increase in brain-to-heart connectivity was detected for theta, alpha, and beta bands during idioventricular rhythms compared with junctional escape rhythms (Fig. 8*B*, *f*). For cortical feedback connectivity, higher values were associated with junctional rhythms than with the ventricular rhythms (Fig. 8*B*, *d* and *f*). These data clearly demonstrate that worsening of cardiac function is strongly associated with increasingly tightened electrical communication and elevated effective connectivity between the brain and heart during asphyxia-induced cardiac arrest.

Blockade of Efferent Input Markedly Delays the Onset of Cardiac Asystole and Prolongs Cortical Coherence. The massive and orderly release of a large set of neurotransmitters from the brain (Fig. 4 and Fig. S4) and increasing functional (Figs. 6 and 8) and effective (Figs. 7 and 8) corticocardiac connectivity during asphyxia prompted us to examine the role of the brain in the rapid demise of the heart. The brain affects cardiac function via the preganglionic sympathetic nerves as well as the vagus nerve. To disconnect the heart from the efferent signals from the brain, we performed spinal cord transection at cervical level 7 (C7) with or without simultaneous blockade of parasympathetic action using atropine before asphyxia. EKG signals persisted more than twice

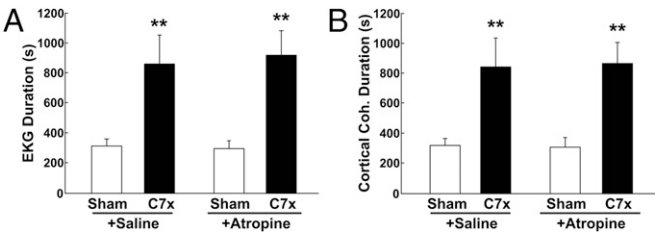

Fig. 9. Blockade of brain's input to the heart prolongs the survival of both the heart and brain during asphyxic cardiac arrest. Rats that received sham surgery or C7 transection surgery were treated without or with atropine (10 mg/kg, i.p.) 30 min before the onset of asphyxia. EKG duration (from the onset of asphyxia to the end of ventricular tachycardia) was 310.6 (SD = ±51.15) s in sham-operated rats, 857.6 (SD = ±195.5) s in C7x rats, 295.8 (SD = ±54.64) s in sham rats with atropine (10 mg/kg) preinjection, and 913.2 (SD = ±169.6) s in C7x rats with atropine treatment (*A*). The duration of mean cortical coherence was 318.4 (SD = ±46.93) s in sham-operated rats, 839.8 (SD = ±192.6) s in C7x rats, 308.4 (SD = ±63.08) s in sham rats with atropine (10 mg/kg) preinjection, and 864. (SD = ±140.2) s in C7x rats with atropine treatment (*B*). Five rats were tested in each cohort. Significant ($P < 0.01$) increases in EKG signal duration (*A*) and mean cortical coherence (*B*) were found in rats with C7 transection, compared with sham-operated rats, and this effect was independent of atropine treatment.

as long in C7x (C7 transection) rats than in sham-operated rats, and atropine did not further enhance this beneficial effect of C7x ($P < 0.01$; Fig. 9*A*). The lengthened cardiac survival by decentralization of the heart also resulted in significantly longer-lasting cortical coherence, and this effect was independent of atropine ($P < 0.01$; Fig. 9*B*). These data suggest that asphyxia-stimulated brain signaling, mediated mainly by the sympathetic nervous system, severely shortens functional activity of the heart and the brain in dying animals.

Discussion

These data demonstrate that asphyxia induces a robust and sustained surge of functional and effective cortical connectivity, an immediate surge of cortical release of a large set of critical neurotransmitters, and delayed activation of corticocardiac (between the cortex and the heart) functional and effective connectivity that persists until the onset of ventricular fibrillation. We showed that blocking autonomic outflow from the brain significantly lengthened survival time of the heart and potentiated persistence of cortical activities despite the continued lack of oxygen. These results demonstrate that asphyxia activates a programmed brainstorm that is coupled to cardiac rhythmicity and accelerates the death of the heart and the brain.

Cardiac Death by Asphyxia Progresses in an Orderly Manner. Sentinel abnormalities in the EKG that precede sudden cardiac death in humans range from ventricular fibrillation, ventricular tachycardia (including torsade de pointes), bradycardia, and pulseless electrical activity (1). No reports are currently available that document how EKG signals of a healthy heart become isoelectric beat by beat, in the absence of external interventions. Our study, aided by the newly invented ECM technology, demonstrates an orderly progression of cardiac failure of rats in response to carbon dioxide-mediated asphyxia (Fig. 1). An initial disruption of sinus rhythm during the first few seconds was followed sequentially by a transient recovery of heart rate, second-degree AV block of Mobitz type II, complete AV block with bradyarrhythmia, junctional escape and ventricular escape (or idioventricular) rhythms, polymorphic ventricular tachycardia, ventricular fibrillations, and finally asystole. Despite continued oxygen deprivation, the heart rate underwent several rounds of ups and downs during asphyxia (Fig. 1 and Fig. S1): (*i*) the initial and rapid drop of heart rate was followed by an equally rapid recovery of heart rate during the first 20 s; (*ii*) the transition from the second- to third-degree AV blocks was accompanied by a sharp drop in heart rate, which subsequently showed an incomplete but significant recovery during early A3; and (*iii*) transition from the junctional escape rhythms to idioventricular rhythms was associated with a further drop of heart rate, which again exhibited some degree of recovery during the late A3. These data support the notion that cardiac activity is under the influence of the autonomic nervous system even during asphyxic cardiac arrest.

Asphyxia Triggers Brainstorm of Coordinated Activity. Cardiac arrest is invariably associated with the loss of external consciousness and sensory responsiveness, which has been interpreted to represent arrested brain function. The extremely low amplitude of scalp EEG, in addition, has been used frequently as evidence for the absolute absence of cortical function during cardiac arrest (22–24). Contrary to this belief, we show here that mammalian brain is highly activated at near-death. In fact, during cardiac arrest, many aspects of cortical activities are much more robust than during waking states. These include (*i*) the marked and global surge of neurophysiological coherence in multiple frequency bands and especially in the gamma-1 band (25–55 Hz) within the cortex; (*ii*) the surge of feedforward and feedback directed connectivity within the cortices especially in theta (5–10 Hz) and gamma-1 bands; (*iii*) an immediate and large surge of orderly release of multiple neurotransmitters in both frontal and occipital cortices; (*iv*) a surge of cardiac event-related potentials that exhibit left–right asymmetry in the cortex; (*v*) a surge of previously unknown neurophysiological coherence between the cerebral cortex and the heart at multiple frequency bands; and (*vi*) progressive elevation of feedforward and feedback cortico-cardiac connectivity for alpha, beta, and gamma-1 bands even in the face of inexorable cardiac failure. Each of these cortical features was active even when intracortical EEG amplitudes fell below 5% of normal levels. These results demonstrate that asphyxia triggers an increase in coordinated cortical activity and that the associated decrease in raw EEG (scalp or intracortical) signal amplitude is a poor indicator of cortical function (25–28).

Indices of Conscious Information Processing Surge During Asphyxic Cardiac Arrest. The global surge of synchronized cortical gamma activities stimulated by asphyxia signifies an internally aroused brain and supports the concept that the mammalian brain is capable of high levels of internal information processing at near-death (9). Functional and effective connectivity in multiple frequency bands, including gamma-1 oscillations, was markedly elevated during the entire period of asphyxic cardiac arrest. The rapid and sustained surge of a large set of core neurotransmitters within the cortex in response to asphyxia provides neurochemical substrates for the elevated information processing in the brain. Norepinephrine, for instance, whose frontal cortex release exhibited more than 30-fold elevation within the first minute of asphyxia, acts centrally to increase alertness, arousal, and attentional performance (29–31). Cortical dopamine, whose release surged more than 12-fold within the first minute of asphyxia, plays important roles in arousal, attention, cognition, and affective emotion (32, 33). Additionally, elevated signaling of both norepinephrine and dopamine contributes to the arousal-promoting actions of psychostimulants (34, 35). Serotonin, whose release in the occipital cortex surged more than 20-fold within the first 2 min of asphyxia, plays diverse central functions via serotonin receptors. Activation of a subset of serotonin receptors, for instance, induces visual hallucinations with mystical feelings in humans (36). Internally generated visions and perceptions apparently occur during cardiac arrest in 10–20% of survivors (22, 24, 37). Although detailed neuronal mechanisms of these realer-than-real (38) near-death experiences remain elusive, our study suggests that the mammalian brain possesses a high capacity for producing well-organized neurophysiological and neurochemical activities and for generation of internal states of consciousness at near-death.

Asphyxia Stimulates a Surge of Asymmetric Cardiac Event-Related Potentials. In this study, a persistent cardiac event-related potential dominated the advanced stages of asphyxia-induced cardiac arrest in all six cerebral cortices in dying animals. Cardiac event-related potential amplitudes on the left hemisphere during cardiac arrest were significantly higher than on the right hemisphere. In humans, the right cerebral cortex is associated with sympathetic functions that convey stress and anxiety responses, and the left cortex controls parasympathetic activity mediating pleasant feelings (39, 40). Afferent neurotransmission from the heart is associated with heartbeat-evoked potentials (41) and represents cortical processing of cardiac afferent input (41–43). Studies indicate that subjectively experienced feelings and emotions could be based on cortical representations of afferent activity in the human brain (33, 40, 44). Furthermore, in our experiment, dopamine release exhibited a more than sevenfold increase in both frontal and occipital lobes within the first minute of asphyxia, and this release exhibited further increase to more than 20-fold over the baseline levels globally in the brain during the late stage of asphyxia. Studies indicate that elevated release of dopamine is associated with positive affective states (45, 46), and hemispheric

asymmetry was reported for the dopaminergic pathways with the left hemisphere favored over the right hemisphere (47). The left hemisphere is more active during feelings of love and maternal attachment (40, 48, 49), whereas the right hemisphere is more active during feelings of stress and anxiety (40). Many cardiac arrest survivors report positive near-death experiences with pleasant and peaceful feelings paradoxically during their unconscious period (22, 37, 50). Our new data provide a neurophysiological framework for understanding the positive feelings (51) reported by cardiac arrest survivors.

Asphyxia-Induced Cardiac Failure Is Associated with Elevated Corticocardiac Coupling. The efferent homeostatic control of cardiac physiology is mediated by the sympathetic and parasympathetic nervous systems in the brainstem and the hypothalamus. Stimulation of locus coeruleus noradrenergic neurons leads to activation of GABAergic inhibition of parasympathetic cardiac vagal neurons via the activation of brainstem adrenergic receptors (14). In our studies, extracellular release of GABA and norepinephrine increased more than 20-fold within the first minute of asphyxia in both frontal and occipital lobes. The elevated norepinephrine release in response to asphyxia is predicted to act within the brainstem to inhibit parasympathetic cardiac vagal neurons. Serotonin released from the raphe complex serves vital functions in the regulation of cardiovascular reflexes, controlling changes in parasympathetic drive to the heart (52). Overexpression of a serotonin auto receptor in raphe nuclei results in sporadic autonomic dysregulation including bradycardia (15). Serotonin release surged more than 70-fold in frontal lobe and 20-fold in occipital lobe within 2 min of asphyxia in our study. The global and dramatic increase of brain serotonin release may exert a powerful influence on cardiovascular reflexes and precipitate a catastrophic autonomic crisis in asphyxic animals.

Parallel to the remarkable central release of the large set of neurotransmitters, bidirectional neurotransmission between the brain and heart also intensified. During asphyxia, top-down efferent neuronal information processing from the cortex to the heart and bottom-up afferent signaling from the heart to the cortex escalated quickly as cardiac conditions deteriorated from junctional escape beats to ventricular escape beats (Fig. 8) and from bradyarrhythmia to ventricular tachycardia (Fig. 7). During each period, the highest feedback connectivity was associated with the highest heart rates. For ID5768, for instance, markedly elevated theta feedback connectivity was seen when the first recovery of heart rate occurred at 20–30 s of asphyxia; the mild increase in heart rate during junctional escape rhythms was associated with increased feedback connectivity in both delta and theta bands (Figs. 1 and 7); the moderate peak of heart rate during idioventricular rhythms was associated with elevated connectivity in theta, alpha, and beta bands; and the highest connectivity values for all frequency bands were detected when heart rate reached its highest levels during ventricular tachycardia. These data indicate that rapid deterioration of cardiac conditions during asphyxia is strongly associated with escalating corticocardiac coupling and suggest that heightened efferent signaling could aggravate the cardiac arrhythmia during asphyxia.

Brain Signaling at Near-Death Accelerates Cardiac Demise. Sudden death can occur as a result of a life-threatening stressor in humans with previously normal heart and brain function (3, 53). The sympathetic nervous system affects cardiac (and other visceral) functions below the spinal segment T1 via the intermediolateral columns of the spinal cord. The parasympathetic nervous system affects cardiac function via the release of acetylcholine from the vagus nerve. Pretreatment with C7 transection (which terminates all sympathetic outflows traveling down the spinal cord) resulted in a nearly threefold increase in cardiac survival time (or EKG signal duration) and duration of detectable cortical coherence compared with the sham operations. In the tested rats, atropine cotreatment did not provide additional benefits. These data are consistent with the idea that autonomic toxicity, induced by a life-threatening crisis, accelerates a rapid demise of the heart (3) and suggest that pharmacological blockade of efferent inputs to the heart may lead to an increased survival of cardiac arrest patients.

Materials and Methods

Animals. Outbred Wistar rats from Harlan were acclimatized in our housing facility for at least 1 wk before surgical implantation of electrodes. Following electrode implantation, rats were allowed to recover for 1 wk before online recording. On the morning of the terminal study and 2 h before the terminal asphyxia induction, a subset of animals was subjected to cord transection at the level of cervical 7 (C7) with a sterile razor blade as the cutting instrument under isoflurane anesthesia. Sham-operated animals (no neural tissue damage) were also used. The experimental procedures were approved by the University of Michigan Committee on Use and Care of Animals. All experiments were conducted using adult rats (300–400 g) maintained on a light:dark cycle of 12:12 h (lights on at 6:00 AM) and provided with ad libitum food and water.

Electrode Implantation and Configuration. Rats were implanted with electrodes for EEG recordings under surgical anesthesia (1.8% isoflurane). The EEG signals were recorded through the screw electrodes implanted bilaterally in the frontal (AP: +3.0 mm; ML: ±2.5 mm, bregma), parietal (AP: −4.0 mm; ML: ±2.5 mm, bregma), and occipital (AP: −8.0 mm; ML: ±2.5 mm, bregma) cortices. The electromyogram (EMG) and EKG were recorded through flexible, insulated (except at the tip) multistranded wires (Cooner Wires) inserted into the dorsal nuchal muscle (EMG) and s.c. muscles flanking the heart (EKG). The EEG, EMG, and EKG electrodes were interfaced with two six-pin pedestals (Plastics One), and the entire assembly was secured on the skull using dental acrylic.

Signal Acquisition. Before the data collection, rats were acclimatized in recording chamber. Electrophysiological signals were recorded using Grass Model 15LT physiodata amplifier system (15A54 Quad amplifiers, Astro-Med, Inc.) interfaced with a BIOPAC MP-150 data acquisition unit and Acqknowledge (version 4.1.1) software (BIOPAC Systems, Inc.). The signals were filtered between 0.1 and 300 Hz and sampled at 1,000 Hz. EEG/EMG/EKG recording was initiated consistently at 10:00 AM to control for circadian factors. Baseline (waking consciousness) EEG signals were recorded for 60 min. At the end of this minimum 1 h of baseline recording, asphyxia cardiac arrest was induced by inhalation of carbon dioxide for 2 min beginning at time 0 s. Recording was continued for an additional 30 min after the onset of asphyxia.

Microdialysis and LC-MS Analysis of Cortical Neurochemicals. Two linear transcranial microdialysis probes (membrane cutoff of 13 kDa) were surgically implanted in each rat in the frontal (AP: +3.0 mm; depth of 2.5 mm) and occipital (AP: −6.5 mm; depth of 2.0 mm) lobes of adult Wistar rats at least 2 d before planned studies. Microdialysis was performed with artificial CSF solution containing 250 μM ascorbate flowing at 2 μL/min with the aid of syringe pump and five-channel liquid swivels, which has a dead volume error of ±1 μL (Instech). With the pump speed of 2 μL/min, the estimated time of events would produce a 30-s error range. Dialysates collected in 1-min bins were derivatized for further analysis (*SI Text*). To capture an array of neurochemicals, we applied a variation of LC-MS analysis (21). Additional details about analysis can be found in *SI Text*.

Signal Analysis Summary. For construction of the EKG matrix (Fig. 1*D*) and EEG matrix (Fig. 5*C*), the preliminary step is the detection of EKG R peaks using variable threshold method, and epochs centered on these R peaks were extracted from the EKG or EEG signals, which were sorted in order of R-peak time to form a colored rectangular image. For mean coherence of six EEG channels (Fig. 2) or between EKG and each of the six EEG channels (Fig. 6), electrical signals were segmented into 2-s epoch with 1 s overlapping over all recorded signals. For each 2-s epoch, mean coherence was calculated based on magnitude squared coherence estimate using Welch's averaged periodogram method with 0.5-Hz frequency bin. The directed connectivity of EEG signals between frontal and posterior (parietal and occipital) brain regions (Fig. 3) or between EKG signal and each of the EEG signals (Fig. 7) was measured by normalized symbolic transfer entropy (NSTE), which quantifies the causal relationship between two electrical signals in each direction. Additional details about analysis can be found in *SI Text*.

ACKNOWLEDGMENTS. We thank Drs. Louis D'Alecy, Jose Jalife, and Anatoli Lopatin for helpful discussions on cardiac physiology; Dr. UnCheol Lee for input on signal processing methods; and Mr. Drew Bennett for discussions on the electrocardiomatrix technology. This work was supported by the Department of Molecular and Integrative Physiology at the University of Michigan, National Institutes of Health Grants R25HL108842 (to J.B.) and R37EB003320 (to R.T.K.), Department of Veterans Affairs Grant I01RX000531 (to M.M.W.), and Michigan Institute on Clinical and Health Research Grant UL1TR000433 (to O.S.M.).

1. Israel CW (2014) Mechanisms of sudden cardiac death. *Indian Heart J* 66(Suppl 1):S10–S17.
2. Cannon WB (1942) "Voodoo" death. *Am Anthropol* 44(2):169–181.
3. Samuels MA (2007) The brain-heart connection. *Circulation* 116(1):77–84.
4. Sörös P, Hachinski V (2012) Cardiovascular and neurological causes of sudden death after ischaemic stroke. *Lancet Neurol* 11(2):179–188.
5. Komura S, Fujimura K (1974) Heart rate and fatal course in rabbits asphyxiated by respiratory arrest. *Tohoku J Exp Med* 114(3):273–275.
6. Ikeda N, Harada A, Suzuki T (1992) The course of respiration and circulation in death due to typical hanging. *Int J Legal Med* 104(6):313–315.
7. Coenen AML, Drinkenburg WHIM, Hoenderken R, van Luijtelaar ELJM (1995) Carbon dioxide euthanasia in rats: Oxygen supplementation minimizes signs of agitation and asphyxia. *Lab Anim* 29(3):262–268.
8. Suzuki T (1996) Suffocation and related problems. *Forensic Sci Int* 80(1-2):71–78.
9. Borjigin J, et al. (2013) Surge of neurophysiological coherence and connectivity in the dying brain. *Proc Natl Acad Sci USA* 110(35):14432–14437.
10. Vaseghi M, Shivkumar K (2008) The role of the autonomic nervous system in sudden cardiac death. *Prog Cardiovasc Dis* 50(6):404–419.
11. Borovsky V, Herman M, Dunphy G, Caplea A, Ely D (1998) CO2 asphyxia increases plasma norepinephrine in rats via sympathetic nerves. *Am J Physiol* 274(1 Pt 2):R19–R22.
12. Meredith IT, Broughton A, Jennings GL, Esler MD (1991) Evidence of a selective increase in cardiac sympathetic activity in patients with sustained ventricular arrhythmias. *N Engl J Med* 325(9):618–624.
13. Cechetto DF (2014) Cortical control of the autonomic nervous system. *Exp Physiol* 99(2):326–331.
14. Wang X, Piñol RA, Byrne P, Mendelowitz D (2014) Optogenetic stimulation of locus ceruleus neurons augments inhibitory transmission to parasympathetic cardiac vagal neurons via activation of brainstem α1 and β1 receptors. *J Neurosci* 34(18):6182–6189.
15. Audero E, et al. (2008) Sporadic autonomic dysregulation and death associated with excessive serotonin autoinhibition. *Science* 321(5885):130–133.
16. Critchley HD, Corfield DR, Chandler MP, Mathias CJ, Dolan RJ (2000) Cerebral correlates of autonomic cardiovascular arousal: A functional neuroimaging investigation in humans. *J Physiol* 523(Pt 1):259–270.
17. Kern M, Aertsen A, Schulze-Bonhage A, Ball T (2013) Heart cycle-related effects on event-related potentials, spectral power changes, and connectivity patterns in the human ECoG. *Neuroimage* 81(C):178–190.
18. Gray MA, et al. (2007) A cortical potential reflecting cardiac function. *Proc Natl Acad Sci USA* 104(16):6818–6823.
19. Lee L, Harrison LM, Mechelli A (2003) A report of the functional connectivity workshop, Dusseldorf 2002. *Neuroimage* 19(2 Pt 1):457–465.
20. Lee U, et al. (2009) The directionality and functional organization of frontoparietal connectivity during consciousness and anesthesia in humans. *Conscious Cogn* 18(4): 1069–1078.
21. Song P, Mabrouk OS, Hershey ND, Kennedy RT (2012) In vivo neurochemical monitoring using benzoyl chloride derivatization and liquid chromatography-mass spectrometry. *Anal Chem* 84(1):412–419.
22. van Lommel P, van Wees R, Meyers V, Elfferich I (2001) Near-death experience in survivors of cardiac arrest: A prospective study in the Netherlands. *Lancet* 358(9298): 2039–2045.
23. Parnia S, Fenwick P (2002) Near death experiences in cardiac arrest: Visions of a dying brain or visions of a new science of consciousness. *Resuscitation* 52(1):5–11.
24. Greyson B (2003) Incidence and correlates of near-death experiences in a cardiac care unit. *Gen Hosp Psychiatry* 25(4):269–276.
25. Bardy AH (2002) Near-death experiences. *Lancet* 359(9323):2116.
26. Tao JX, Ray A, Hawes-Ebersole S, Ebersole JS (2005) Intracranial EEG substrates of scalp EEG interictal spikes. *Epilepsia* 46(5):669–676.
27. Kobayashi E, Hawco CS, Grova C, Dubeau F, Gotman J (2006) Widespread and intense BOLD changes during brief focal electrographic seizures. *Neurology* 66(7):1049–1055.
28. French CC (2009) Near-death experiences and the brain. *Psychological Scientific Perspectives on Out-of-Body and Near-Death Experiences* (Nova Science Publishers, Hauppauge, NY), pp 187–204.
29. Foote SL, Berridge CW, Adams LM, Pineda JA (1991) Electrophysiological evidence for the involvement of the locus coeruleus in alerting, orienting, and attending. *Prog Brain Res* 88:521–532.
30. Berridge CW, Schmeichel BE, España RA (2012) Noradrenergic modulation of wakefulness/arousal. *Sleep Med Rev* 16(2):187–197.
31. Szabadi E (2013) Functional neuroanatomy of the central noradrenergic system. *J Psychopharmacol* 27(8):659–693.
32. Aalto S, Brück A, Laine M, Någren K, Rinne JO (2005) Frontal and temporal dopamine release during working memory and attention tasks in healthy humans: A positron emission tomography study using the high-affinity dopamine D2 receptor ligand [11C]FLB 457. *J Neurosci* 25(10):2471–2477.
33. Clark KL, Noudoost B (2014) The role of prefrontal catecholamines in attention and working memory. *Front Neural Circuits* 8:33.
34. Berridge CW (2006) Neural substrates of psychostimulant-induced arousal. *Neuropsychopharmacology* 31(11):2332–2340.
35. Berridge CW, Arnsten AFT (2013) Psychostimulants and motivated behavior: Arousal and cognition. *Neurosci Biobehav Rev* 37(9 Pt A):1976–1984.
36. Rolland B, et al. (2014) Pharmacology of hallucinations: Several mechanisms for one single symptom? *BioMed Res Int* 2014(1):1–9.
37. Parnia S, Waller DG, Yeates R, Fenwick P (2001) A qualitative and quantitative study of the incidence, features and aetiology of near death experiences in cardiac arrest survivors. *Resuscitation* 48(2):149–156.
38. Thonnard M, et al. (2013) Characteristics of near-death experiences memories as compared to real and imagined events memories. *PLoS ONE* 8(3):e57620.
39. Wittling W, Block A, Genzel S, Schweiger E (1998) Hemisphere asymmetry in parasympathetic control of the heart. *Neuropsychologia* 36(5):461–468.
40. Craig ADB (2005) Forebrain emotional asymmetry: A neuroanatomical basis? *Trends Cogn Sci* 9(12):566–571.
41. Schandry R, Montoya P (1996) Event-related brain potentials and the processing of cardiac activity. *Biol Psychol* 42(1-2):75–85.
42. Critchley HD, Harrison NA (2013) Visceral influences on brain and behavior. *Neuron* 77(4):624–638.
43. Craig AD (2003) Interoception: The sense of the physiological condition of the body. *Curr Opin Neurobiol* 13(4):500–505.
44. Critchley HD, et al. (2005) Mental stress and sudden cardiac death: Asymmetric midbrain activity as a linking mechanism. *Brain* 128(Pt 1):75–85.
45. Ashby FG, Isen AM, Turken AU (1999) A neuropsychological theory of positive affect and its influence on cognition. *Psychol Rev* 106(3):529–550.
46. Burgdorf J, Panksepp J (2006) The neurobiology of positive emotions. *Neurosci Biobehav Rev* 30(2):173–187.
47. Tucker DM, Williamson PA (1984) Asymmetric neural control systems in human self-regulation. *Psychol Rev* 91(2):185–215.
48. Bartels A, Zeki S (2004) The neural correlates of maternal and romantic love. *Neuroimage* 21(3):1155–1166.
49. Leibenluft E, Gobbini MI, Harrison T, Haxby JV (2004) Mothers' neural activation in response to pictures of their children and other children. *Biol Psychiatry* 56(4): 225–232.
50. Parnia S, et al. (2014) AWARE-AWAreness during REsuscitation-a prospective study. *Resuscitation* 85(12):1799–1805.
51. Charland-Verville V, et al. (2014) Near-death experiences in non-life-threatening events and coma of different etiologies. *Front Hum Neurosci* 8:203.
52. Ramage AG, Villalón CM (2008) 5-hydroxytryptamine and cardiovascular regulation. *Trends Pharmacol Sci* 29(9):472–481.
53. Sharkey SW, Lesser JR, Maron BJ (2011) Cardiology Patient Page. Takotsubo (stress) cardiomyopathy. *Circulation* 124(18):e460–e462.